

Power-Law Creep from Discrete Dislocation Dynamics

Shyam M. Keralavarma,¹ T. Cagin,^{2,3} A. Arsenlis,⁴ and A. Amine Benzerga^{1,2,*}

¹Department of Aerospace Engineering, Texas A&M University, College Station, Texas 77843, USA

²Materials Science and Engineering Program, Texas A&M University, College Station, Texas 77843, USA

³Department of Chemical Engineering, Texas A&M University, College Station, Texas 77843, USA

⁴Lawrence Livermore National Laboratory, Livermore, California 94551, USA

(Received 4 September 2012; revised manuscript received 3 November 2012; published 26 December 2012)

We report two-dimensional discrete dislocation dynamics simulations of combined dislocation glide and climb leading to “power-law” creep in a model aluminum crystal. The approach fully accounts for matter transport due to vacancy diffusion and its coupling with dislocation motion. The existence of quasiequilibrium or jammed states under the applied creep stresses enables observations of diffusion and climb over time scales relevant to power-law creep. The predictions for the creep rates and stress exponents fall within experimental ranges, indicating that the underlying physics is well captured.

DOI: [10.1103/PhysRevLett.109.265504](https://doi.org/10.1103/PhysRevLett.109.265504)

PACS numbers: 61.72.Bb, 46.35.+z, 62.20.Hg, 91.60.Dc

Dislocations are the main carriers of deformation in crystal plasticity [1]. The glide motion of these line defects dominates at low homologous temperatures, whereas their climb, a nonconservative motion mediated by the absorption or emission of lattice vacancies, becomes important in high-temperature deformation (creep) [2]. It is generally believed that the creep strain is mainly produced by dislocation glide at a rate set by dislocation climb [2,3]. However, a detailed analysis of the phenomenon is lacking due to the complexity of incorporating both vacancies and dislocations in a single computational framework. As a thermally activated process, the diffusion of vacancies occurs over time scales that are much longer than can be accessed by molecular dynamics [4,5], and available dislocation dynamics formulations [6–9] do not account for the nonlinear vacancy-dislocation interactions inherent to climb [3,10]. Only recently have dislocation glide and climb been simultaneously considered in the simulation of prismatic loop coarsening [11]. In this Letter, we extend this approach to simulate power-law creep. The approach fully utilizes quasiequilibrium or “jammed” dislocation states under the low creep stresses to effectively bridge the fine time scales of dislocation glide with the coarse time scales of diffusion-controlled climb in a single simulation. It also employs a variational principle to derive boundary conditions for the coupled problem and a dislocation climb model with atomistic fidelity [3].

When the climb motion of noninteracting, pinned edge dislocation segments normal to the slip plane is assumed to proceed at a velocity proportional to the applied stress (σ) [12,13], the steady-state creep rate exhibits a power-law stress dependence $\dot{\epsilon} \propto \sigma^n$ with $n = 3$ [14]. If glide is considered in a creep model, Weertman has shown that the stress exponent increases to $n = 4.5$; see Ref. [15] and references therein. In fact, the exponent is between 4 and 8 from experiments [16], which hints at more complex glide-climb couplings in dislocation creep. Interestingly, recent

atomistic simulations, based on a kinetic Monte Carlo scheme, and accounting only for climb, yielded $n \approx 5$ in bcc iron [10]. However, when this prediction is extrapolated to lower, realistic dislocation densities and applied stress levels, n is found to be no more than 3.5 [3], consistent with any creep model based on pure climb [15]. Here, we also explore the extent to which the explicit consideration of both climb and glide delivers experimentally reported stress exponents.

In the current literature, three-dimensional discrete dislocation dynamics formulations of coupled glide and climb remain scarce [11] and do not address creep predictions. Some of the remaining challenges involve bridging the disparate time scales and incorporating a precise coupling between elasticity and diffusion. Therefore, the investigation of creep is of considerable importance, but even in two dimensions (2D), this problem has not been solved yet.

We consider a simplified 2D model specimen subjected to plane strain uniaxial loading at constant average stress with traction-free top and bottom surfaces, Fig. 1(a). The specimen initially contains discrete edge dislocations, dislocation sources, and obstacles embedded in a linear elastic material. The instantaneous state of the system is characterized by the positions of all dislocations, $\mathbf{x}^i(t)$ ($i = 1, 2, 3, \dots$), and a continuous field of the fractional vacancy concentration, $c(\mathbf{x}, t)$. The long- and short-range dislocation interactions are handled as in Refs. [17,18] using the finite-element method. The driving force for dislocation motion is the generalized Peach-Koehler force while the driving force for vacancy diffusion is the gradient of the chemical potential μ , both of which may be obtained from derivatives of the Gibbs free-energy function $G(\mathbf{x}^i, c)$. The governing equations for vacancy diffusion are

$$\dot{c} = -\nabla \cdot \mathbf{J} + \dot{c}_{\text{src}}, \quad (1)$$

$$\mathbf{J} = -\frac{D\Omega}{kT} \nabla \mu, \quad (2)$$

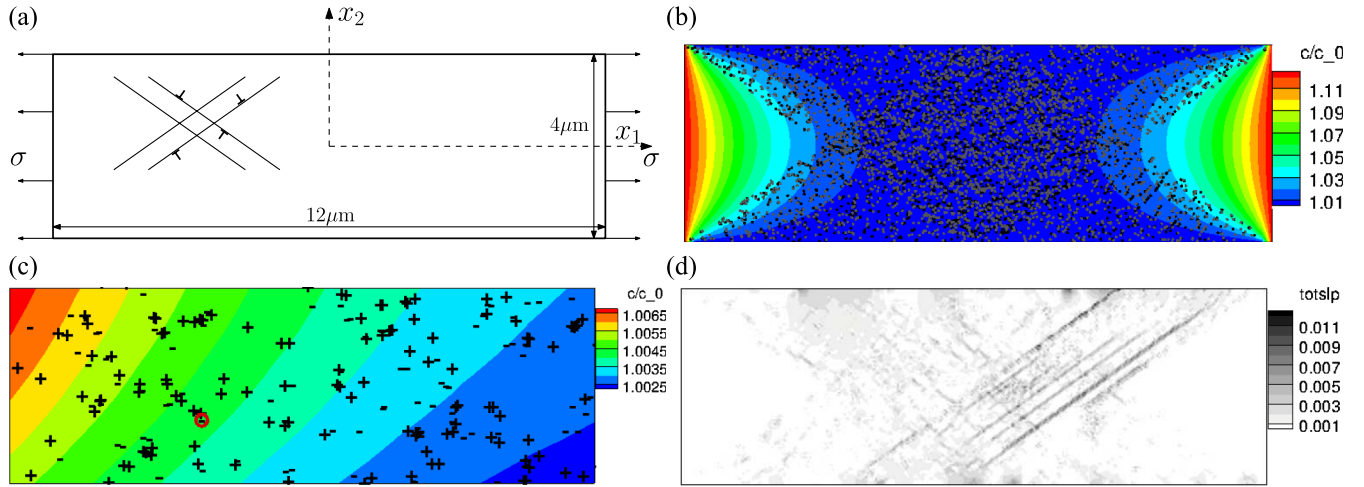


FIG. 1 (color online). (a) Sketch of computational specimen containing discrete edge dislocations on two independent slip systems oriented at $\pm 35.25^\circ$ with respect to the axis of loading (horizontal). (b) Contours of vacancy concentration superposed on the positions of dislocations (positive: black; negative: gray) before the first climb event in a creep simulation ($\sigma = 40$ MPa, $T = 400$ K). (c) Magnified view of a $1.5 \times 0.5 \mu\text{m}$ region around the climbing dislocation (red circle). (d) Typical contours of slip over a time interval of 200 s around $t = 4000$ s in the same creep simulation.

$$\mu = \frac{kT}{\Omega} \left[\frac{E_f}{kT} - \frac{p\Omega_v}{kT} + \log \frac{c}{(1-c)} \right]. \quad (3)$$

Equation (1) follows from mass conservation where \mathbf{J} denotes the volumetric flux of vacancies and \dot{c}_{src} is a production term (see below). In Eqs. (2) and (3), k is Boltzmann's constant, T the absolute temperature, Ω the atomic volume, E_f the vacancy formation energy, $p = p(\mathbf{x}, t)$ denotes the hydrostatic pressure field, Ω_v the vacancy relaxation volume, and $D = D_0 \exp(-\frac{E_m}{kT})$ the vacancy diffusion coefficient, with E_m the vacancy migration energy. In the absence of pressure gradients, Eq. (2) reduces to Fick's first law of diffusion. The glide velocity v_g^i of dislocation i is taken to be proportional to the glide component of the Peach-Koehler force f_g^i , as

$$v_g^i = f_g^i / B(T), \quad (4)$$

where the drag factor B varies linearly with temperature [13]. In the most fundamental formulation, the climb velocity v_c^i is determined by mass conservation from $b^i v_c^i = \int_{\partial C^i} \mathbf{J} \cdot \mathbf{n} dS$, where ∂C^i denotes the dislocation core boundary with inward unit normal \mathbf{n} , so that $\dot{c}_{\text{src}} = 0$ in (1). To circumvent the computational complexity of such an approach, v_c^i is estimated from the *net* flux of vacancies to and from the dislocation core and mass conservation, over a larger volume under steady-state climb conditions and assumed radial symmetry around the core [13,19]

$$v_c^i = -\eta \frac{D}{b^i} \left[c_0 \exp\left(-\frac{f_c^i \Omega}{b^i kT}\right) - c \right]. \quad (5)$$

The first term in brackets is the concentration of vacancies in equilibrium with the core, where f_c^i denotes the climb component of the Peach-Koehler force, b^i is the magnitude

of the Burgers vector, and $c_0 = \exp(-E_f/kT)$ is the equilibrium vacancy concentration in a bulk material at temperature T . c is the ambient vacancy concentration away from the dislocation core, here obtained from the solution of the global diffusion equations interpolated to the dislocation position under the assumption that the dislocation core radius is much smaller than the length scale of the gradients of c . η is a constant of order unity. As shown in Ref. [3], the performance of analytical estimate (5) against atomistic simulations is remarkable. Consistent with this, the term \dot{c}_{src} is added to (1) to account for the net absorption or emission of vacancies in the volume element.

In order to perform creep simulations over time durations sufficient to establish a steady state, we used an adaptive scheme to increment the simulation time step proceeding as follows. We first relaxed the initial dislocation microstructures at zero stress until the dislocations attained quasiequilibrium positions. Thereafter, we applied the creep stress (below the nominal yield stress of the specimen) and performed the simulation using a small time step of 0.5 ns to resolve glide-related events until the overall strain attained a constant value as determined by measuring the average slope of the strain versus time plot over a predefined interval. Attainment of such a “jammed” or quasiequilibrium state enables observation of creep deformation over macroscopically relevant time scales. Indeed, at that point, we computed the evolution of the vacancy field by solving Eqs. (1)–(3) using the finite element method and a much larger value of the time step, dependent on temperature as per the analytical estimate (5) for climbing to a neighboring slip plane. Dirichlet boundary conditions were imposed for c corresponding to the equilibrium concentrations at the boundaries consistent

with the imposed tractions. The initial c field was specified according to the steady-state solution of Eq. (1), with $\dot{c} = 0$ and $\dot{c}_{\text{src}} = 0$. Because of the much larger value of the time step used, the diffusion equations are solved using a fully implicit algorithm as opposed to a simple forward Euler scheme for the glide steps. When the first “activation event” is detected, i.e., when any dislocation climbs to a new slip plane thereby enabling further glide, the time step is reverted to the fine 0.5 ns value. Note that the dislocation dynamics (DD) and the vacancy diffusion problems are inherently coupled since the frequency and locations of the dislocation climb events are determined by the vacancy distribution according to Eq. (5) and any production or annihilation of vacancies due to climb affects the evolution of the vacancy field through the production term in Eq. (1).

We performed all simulations using physical properties of fcc aluminum: Young’s modulus $E = 70$ GPa, Poisson’s ratio $\nu = 0.33$, $E_f = 0.67$ eV, $E_m = 0.61$ eV, $D_0 = 1.51 \times 10^{-5}$ m²/s [20]. Also, $B(T) = 10^{-4} \times (T/300)$ Pa s, $\Omega = 16.3 \text{ \AA}^3$, and $b = 0.25$ nm. The relaxation volume of a vacancy in Al is neglected and the geometry factor η in (5) is taken to be unity. The temperature dependence of the elastic properties is neglected. Figure 1(b) shows the dislocation positions before the first climb event in a creep simulation of a $12 \times 4 \mu\text{m}^2$ specimen at $T = 400$ K and $\sigma = 40$ MPa superposed with contours of the normalized vacancy concentration c/c_0 . Figure 1(c) shows a magnified view of a $1.5 \times 0.5 \mu\text{m}^2$ region around the climbing dislocation. Figure 1(d) shows the contours of cumulated plastic slip over a 200 s time interval in the same specimen. Unlike in a plasticity simulation by pure glide, which shows sharp slip traces oriented along the slip planes, Fig. 1(d) shows some bands oriented normal to the slip planes, indicating dislocation climb activity.

A large number of creep simulations have been carried out in the temperature range $T = 400\text{--}800$ K ($0.43T_m\text{--}0.86T_m$, $T_m = 933$ K for Al) and stresses $\sigma = 10\text{--}90$ MPa [spanning the range 10^{-4} G– 10^{-3} G for the resolved shear stress with $G = E/(2(1 + \nu))$ the shear modulus]. Figure 2(a) shows the creep curves obtained from the DD simulations at $T = 400$ K ($0.43T_m$) and several values of the creep stress. The high-temperature DD simulations yield a steady-state creep response with the strain rate increasing with the applied stress. A characteristic feature of steady-state creep is that the material microstructure remains unchanged with time on average. An average description of the microstructure in the present problem is the dislocation density, which is plotted as a function of time in Fig. 2(b) corresponding to the creep curves in Fig. 2(a). Following a rapid initial transient, the dislocation density evolves slowly with time except at high stresses, indicating that steady-state conditions have been attained. The steady-state creep rates depend exponentially on the temperature, and the relationship between the

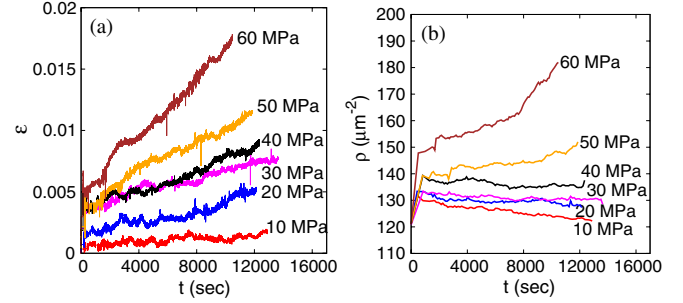


FIG. 2 (color online). (a) Creep curves showing the total strain ϵ as a function of time t for various values of the creep stress at $T = 400$ K. (b) Corresponding evolution of the dislocation density ρ .

creep rates and the temperature follows an Arrhenius-type equation

$$\dot{\epsilon} = \dot{\epsilon}_0 \exp\left(-\frac{Q}{kT}\right), \quad (6)$$

where the activation energy for creep Q is experimentally known to be close to the activation energy for self-diffusion, $E_s = E_f + E_m$. The former may be determined from the negative slope of the logarithm of the strain rate plotted as a function of the reciprocal temperature, as shown in Fig. 3 for various values of the creep stress. Notice that a more or less constant slope is obtained for the activation plot irrespective of the creep stress, and the measured value of $Q = 120$ kJ/mol compares favorably with the value of $E_s = 123$ kJ/mol assumed in the simulations. The emergence of creep from DD simulations [Figs. 2(a) and 3] is the main result of this Letter.

The stress dependence of the creep rate has been probed in the temperature range $T = 400\text{--}800$ K. Figure 4 plots the steady-state creep rates (determined approximately by a linear least-squares fit to the $\epsilon\text{--}t$ plots) as a function of the

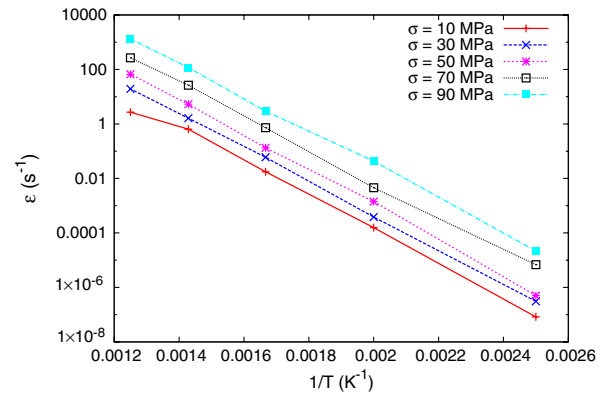


FIG. 3 (color online). Variation of the creep strain rate as a function of reciprocal temperature for various values of the creep stress. The Arrhenius activation energy for creep estimated from the average slopes of the above plots is approximately 120 kJ/mol.

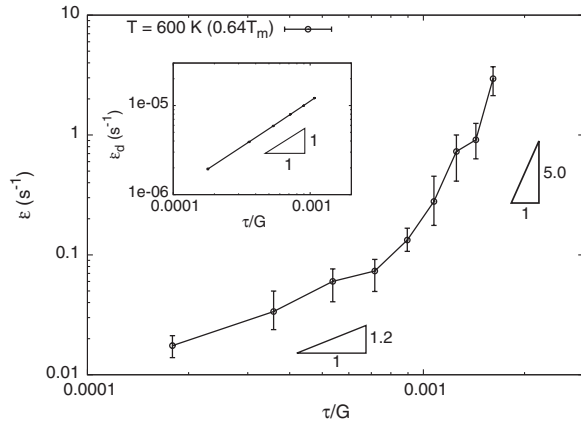


FIG. 4. Scaling of the net creep strain rate $\dot{\epsilon}$ with the normalized resolved shear stress τ/G at $T = 600$ K. The strain rates are averaged over at least three realizations of the initial microstructure, consisting of randomly distributed dislocations, point sources, and obstacles with a specified average density. The creep exponent n is measured as the slope of the curve on the log-log plot. The inset shows the scaling of the creep rate due to vacancy diffusion (Nabarro-Herring creep).

creep stress at $T = 600$ K on a log-log scale and illustrates the typical emergent behavior. A minimum of three sets of simulations have been performed using different realizations of the initial dislocation, source, and obstacle structure for a given value of the creep stress. These attributes of the initial microstructure are chosen so that the nominal yield stress in a displacement driven simulation is ≈ 80 – 90 MPa. The slope of the log-log plot gives the stress exponent n . The results show two distinct regimes where the stress exponent approaches unity towards low values of the creep stress ($\tau \sim 10^{-4}$ G) while $n \approx 5$ is obtained at high stresses ($\tau \sim 10^{-3}$ G).

The creep strain in Fig. 2(a) has two components: one is mechanical that results from dislocation motion, the other is diffusive due to transport of matter towards the loaded ends of the specimen. The average creep rate due to mass transport $\dot{\epsilon}_d$ is estimated as the total volumetric flux of vacancies from the end faces normalized by the volume of the specimen. The inset in Fig. 4 plots just the diffusion component of the creep strain rate $\dot{\epsilon}_d$ as a function of the stress. The latter yields a stress scaling exponent $n = 1$ as expected for the Nabarro-Herring creep mechanism. Also, it is clear that at $T = 600$ K, the diffusion contribution to the overall creep rate is negligible compared to that due to combined dislocation glide and climb. The same qualitative behavior as in Fig. 4 is obtained at all temperatures above $0.4T_m$. Figure 5 summarizes the results of our simulations and shows the measured value of n at low and high stresses as a function of temperature. Values of n close to unity are obtained at low stresses while at high stresses the predicted values of n span the range 5–7, well within the experimental range of 4–8.

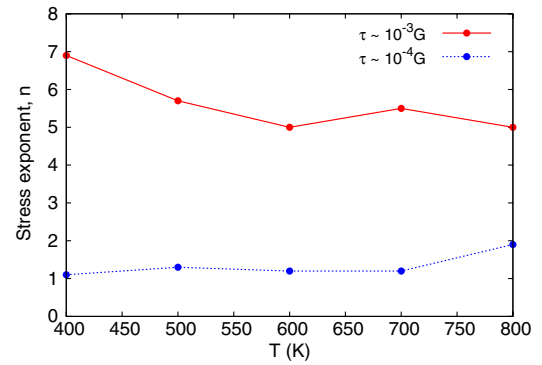


FIG. 5 (color online). Variation of the stress exponent for creep determined from the simulations as a function of temperature for low ($\sim 10^{-4}$ G) and high ($\sim 10^{-3}$ G) values of the creep stress.

The good agreement between the calculated and measured power-law creep exponents is a major result of this Letter. We note, however, that a 2D treatment of dislocation dynamics sets restrictions on (i) the actual degrees of freedom that flexible dislocations have, and (ii) the incorporation of other recovery mechanisms, such as cross slip [21], or bypassing versus shearing of precipitates. It remains to be seen what stress exponents will emerge from fully 3D simulations, properly extended as done here in 2D.

Our results show that mesoscale simulation methods such as DD can provide new insights into aspects of material behavior heretofore not explained using continuum approaches. Unlike fully discrete methods such as molecular dynamics, mesoscale methods offer better scalability to larger and more complex problems. Beyond the athermal interactions of dislocations considered in most DD studies, thermally activated mechanisms of deformation predominate under different regimes of stress and temperature, as illustrated succinctly in deformation mechanism maps [16]. Our results show that power-law exponents of 5 and higher emerge, at realistic levels of stress and dislocation density, when both climb and glide are modeled and that the collective behavior of dislocations, which is not amenable to simple analytical treatment, contributes to the power-law dependence.

We gratefully acknowledge financial support from the Lawrence Livermore National Security, LLC under Master Task Agreement No. B575363, LLNL under Contract No. DE-AC52-07NA27344, and the National Science Foundation under Grant No. CMMI-0748187 (A. A. B.).

*benzerga@tamu.edu

- [1] J. Friedel, *Dislocations* (Pergamon, Oxford, 1964).
- [2] D. Caillard and J. Martin, *Thermally Activated Mechanisms in Crystal Plasticity* (Elsevier Science, Amsterdam, 2003), Vol. 8.
- [3] E. Clouet, *Phys. Rev. B* **84**, 092106 (2011).
- [4] P. Gumbsch and H. J. Gao, *Science* **283**, 965 (1999).

- [5] G.F. Wang, A. Strachan, T. Cagin, and W.A. Goddard, *Phys. Rev. B* **68**, 224101 (2003).
- [6] V. Bulatov, F.F. Abraham, L. Kubin, B. Devincre, and S. Yip, *Nature (London)* **391**, 669 (1998).
- [7] N.M. Ghoniem, S.H. Tong, and L.Z. Sun, *Phys. Rev. B* **61**, 913 (2000).
- [8] V.V. Bulatov, L.L. Hsiung, M. Tang, A. Arsenlis, M.C. Bartelt, W. Cai, J.N. Florando, M. Hiratani, M. Rhee, G. Hommes *et al.*, *Nature (London)* **440**, 1174 (2006).
- [9] D. Gómez-García, B. Devincre, and L.P. Kubin, *Phys. Rev. Lett.* **96**, 125503 (2006).
- [10] M. Kabir, T. T. Lau, D. Rodney, S. Yip, and K. J. Van Vliet, *Phys. Rev. Lett.* **105**, 095501 (2010).
- [11] B. Bakó, E. Clouet, L. M. Dupuy, and M. Blétry, *Philos. Mag.* **91**, 3173 (2011).
- [12] N.F. Mott, *Proc. Phys. Soc. London Sect. B* **64**, 729 (1951).
- [13] J.P. Hirth and J. Lothe, *Theory of Dislocations* (Wiley, New York, 1968).
- [14] J. Weertman, *Jpn. J. Appl. Phys., Suppl.* **26**, 1213 (1955).
- [15] J. Weertman and J.R. Weertman, *Annu. Rev. Earth Planet. Sci.* **3**, 293 (1975).
- [16] H.J. Frost and M.F. Ashby, *Deformation-Mechanism Maps: The Plasticity and Creep of Metals and Ceramics* (Pergamon, Oxford, 1982).
- [17] E. Van der Giessen and A. Needleman, *Model. Simul. Mater. Sci. Eng.* **3**, 689 (1995).
- [18] A.A. Benzerga, Y. Bréchet, A. Needleman, and E. Van der Giessen, *Model. Simul. Mater. Sci. Eng.* **12**, 159 (2004).
- [19] D. Mordehai, E. Clouet, M. Fivel, and M. Verdier, *Philos. Mag.* **88**, 899 (2008).
- [20] P. Freund and K. Heinloth, *Numerical Data and Functional Relationships in Science and Technology: New Series* (Springer, New York, 2002).
- [21] J.P. Poirier, *Rev. Phys. Appl.* **11**, 731 (1976).